OCEANOGRAPHY

Scale of oceanic eddy killing by wind from global satellite observations

Shikhar Rai[1], Matthew Hecht[2], Matthew Maltrud[2], Hussein Aluie[1]*

Wind is the primary driver of the oceanic general circulation, yet the length scales at which this energy transfer occurs are unknown. Using satellite data and a recent method to disentangle multiscale processes, we find that wind deposits kinetic energy into the geostrophic ocean flow only at scales larger than 260 km, on a global average. We show that wind removes energy from scales smaller than 260 km at an average rate of −50 GW, a process known as eddy killing. To our knowledge, this is the first objective determination of the global eddy killing scale. We find that eddy killing is taking place at almost all times but with seasonal variability, peaking in winter, and it removes a substantial fraction (up to 90%) of the wind power input in western boundary currents. This process, often overlooked in analyses and models, is a major dissipation pathway for mesoscales, the ocean's most energetic scales.

INTRODUCTION

It is widely recognized that oceanic circulation is driven primarily by wind (*1*). Although the net path of mechanical energy is from the atmosphere to the ocean, several recent studies have shown evidence that oceanic eddies can actually lose energy to the atmosphere (*2*–*4*) in a process dubbed "eddy killing" (*5*).

Determining the pathways to dissipation of the geostrophic (or balanced) flow is a long-standing problem in physical oceanography (*6*), contributing to large uncertainties in the oceanic kinetic energy budget. Eddy killing by the atmosphere may be an important dissipation pathway for the mesoscales [$O(100)$ km], which constitute a peak in the kinetic energy spectrum (*7*, *8*), are a critical component of the global circulation and its response to changes in atmospheric forcing, and play a leading role in the transport of heat and biogeochemical tracers (*9*–*11*). There are now considerable discrepancies in estimates of wind power input into the mesoscales. Moreover, eddy killing is misrepresented in ocean-only models where the wind is prescribed. Such misrepresentation in ocean-only models has implications on both large and small scales, leading to systematic biases in the modeling of ocean circulation, its turbulence levels, transport, and mixing (*12*–*15*).

The standard explanation of eddy killing is sketched in Fig. 1. It shows a large-scale wind blowing over a small-scale ocean eddy. The wind stress, $\boldsymbol{\tau}$, is proportional to wind velocity relative to the ocean velocity, which induces small-scale oceanic imprints (or variations) onto the wind stress (*3*, *16*). The resultant stress forces half of the eddy positively (positive work) and the other half negatively (negative work or damping). Because the stress is proportional to wind velocity relative to the ocean, the negative forcing dominates over the positive, giving rise to eddy killing as sketched in Fig. 1. In strongly eddying regions such as western boundary currents (WBCs), eddy killing can be an important energy sink and represents a legitimate energy pathway in ocean models (*17*) as we shall show below.

To date, there has been no analysis of the scales at which eddy killing operates in the global ocean. Does wind always damp the mesoscales? It is known, for example, that small-scale currents near land are actually wind-driven rather than damped (*16*, *18*, *19*). Moreover, while wind may damp individual coherent circular eddies of any scale ℓ, as illustrated in Fig. 1, it can still deposit a net positive amount of energy at that scale ℓ when accounting for all other flow structures of size ℓ, such as strain-dominated regions and irregular meanders. Quantifying the net power deposited by wind into the entire mesoscale flow, encompassing all possible structures, is central to determining the eddy killing contribution to the global budget and to understanding what oceanic scales are driven directly by wind. From a modeling perspective, there is an immediate practical utility to quantifying the length scales at which eddy killing operates to guide its proper representation in models at varying grid resolution.

There have been several approaches and definitions for measuring eddy killing, which do not agree in their estimates. Many of the earlier investigations relied on Reynolds (or temporal) averaging (*5*, *18*–*22*), in which "eddy" is the ocean surface velocity deviation, $\boldsymbol{u}_o' = \boldsymbol{u}_o - \langle \boldsymbol{u}_o \rangle$, from the time mean $\langle \boldsymbol{u}_o \rangle$. Consistent with this definition, the measure of wind power input into the eddy (i.e., fluctuating)

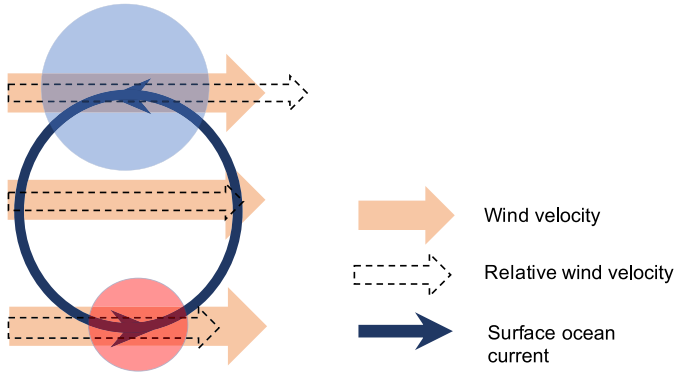

Fig. 1. Standard explanation of eddy killing. A uniform (or large scale) wind acts on an ocean eddy (small scale) (*3*). Wind stress forces the top half of the eddy negatively (blue patch) and the bottom half positively (red patch). Because the stress exerted by wind on the eddy is proportional to their relative velocity, the negative forcing dominates over the positive, resulting in the wind extracting energy from the eddy. Note that eddy killing in this stationary configuration cannot be detected using a time mean and eddy decomposition of the flow.

[1]Department of Mechanical Engineering, University of Rochester, Rochester, NY 14627, USA. [2]Los Alamos National Laboratory, Los Alamos, NM 87545, USA.
*Corresponding author. Email: hussein@rochester.edu

field is $<\boldsymbol{\tau}' \cdot \boldsymbol{u}_o'>$. However, all these studies have found this quantity to be either positive or ≈0 when integrated globally and also in most regions of interest, suggesting (misleadingly) a lack of eddy killing. A conclusion of our study here is that eddy killing is inherently a spatial process that cannot be captured by temporal averaging. A temporal analysis would yield zero eddy killing for the stationary flow configuration in Fig. 1 because it involves no temporal fluctuations.

More recently, Xu *et al.* (*23*) pursued another approach to measure eddy killing by explicitly detecting eddies of size up to 400 km. They found that wind power input, $\boldsymbol{\tau} \cdot \boldsymbol{u}_o^{eddy}$, over such structures is −27.7 GW, where $\boldsymbol{u}_o^{\text{eddy}}$ is the velocity of detected eddies. This measure can be regarded as a lower bound for the eddy killing magnitude because it relies on eddy detection criteria that are ultimately subjective. For example, would an unclosed or irregularly shaped meander be considered an eddy? A third approach to estimate eddy killing was developed in the form of a linear regression coefficient obtained from the empirical correlation of wind stress curl and ocean surface vorticity (*16*, *24*, *25*). Using such a regression coefficient, Renault *et al.* (*25*) estimated global eddy killing to be −48 GW. Yet, regression coefficients are sensitive to the data size and rely on a (spatial and/or temporal) spread in the range of values being statistically correlated. For example, the regression analysis in (*25*) cannot be applied to the flow in Fig. 1 because there are no statistical fluctuations yielding a spread in values. Renault *et al.* (*25*) reported two other measures of eddy killing that yielded −23 and −70 GW in that same study.

While the aforementioned studies have helped shed light on the process of eddy killing, we still lack a first-principles method to quantify it. This is essential given the wide scatter in eddy killing estimates (from +22 to −23 to −70 GW), including positive values that cast doubt on the very existence of eddy killing in the global budget (*18*, *19*, *25*).

Below, we shall quantify global eddy killing from satellite observations using a coarse-graining approach developed recently to probe multiscale geophysical processes (*26*, *27*). We show how we are able to extract a physically correct value of eddy killing by coarse graining at any length scale of choice and calculating the wind work on those scales. By performing a "scan" over an entire range of length scales, we are able to unravel those scales at which eddy killing operates, in addition to its magnitude. We find that wind extracts power from the ocean at scales smaller than 260 km and at an average rate of −50 GW globally. In WBCs, eddy killing is substantial; it removes energy almost equal to total wind work in the Kuroshio, removes 50% of total wind work in the Gulf Stream, and is so strong in the Agulhas that it renders total wind work negative despite the positive power fed into large scales. We also find that eddy killing is persistent year-round; the wind damps scales smaller than 260 km at almost all times, not just on average, and that it exhibits clear seasonal variability, peaking in the winter. Our analysis also indicates that eddy killing is an important dissipation pathway for the mesoscales, acting as a sink ≈60% of the strength of the inverse cascade pathway in the top 100 m of the ocean. By unraveling eddy killing as a function of length scale, our work constitutes a first-principles guide based on observations for how to properly account for eddy killing as a function of grid resolution in numerical models.

RESULTS AND DISCUSSION

The coarse-graining approach, described in Materials and Methods and in (*26*, *27*), allows us to identify the energy deposited by wind stress, $\boldsymbol{\tau}$, into any band of oceanic scales by a simple spatial filtering of the governing dynamics and deriving the corresponding kinetic energy budget. It is then straightforward to show that the "eddy power" (EP) input by wind is

$$EP_\ell^{Cg} = \overline{\boldsymbol{\tau} \cdot \boldsymbol{u}_o} - \overline{\boldsymbol{\tau}} \cdot \overline{\boldsymbol{u}_o} \tag{1}$$

Equation 1 captures the wind's direct contribution to the ocean's kinetic energy at scales smaller than length ℓ, with superscript "Cg" to denote coarse graining. Here, $\overline{\boldsymbol{\tau}}$ and $\overline{\boldsymbol{u}}_o$ are the wind stress and ocean surface velocity, respectively, low-pass–filtered in space (denoted by the overbar, $\bar{\cdot}$) to account for only scales larger than length ℓ. This large-scale contribution, $\overline{\boldsymbol{\tau}} \cdot \overline{\boldsymbol{u}_o}$, is then subtracted from the total wind power input in Eq. 1 to yield the residual small-scale contribution, EP_ℓ^{Cg} (see Materials and Methods).

Quantity EP_ℓ^{Cg} is analogous to that obtained from the commonly used Reynolds averaging approach (*5*, *18*–*20*), which decomposes the flow into a temporal mean and fluctuating components. There, wind power input into the fluctuations (or "eddies") is

$$\mathrm{EP}^{Rey} = <\boldsymbol{\tau} \cdot \boldsymbol{u}_o> - <\boldsymbol{\tau}> \cdot <\boldsymbol{u}_o> = <\boldsymbol{\tau}' \cdot \boldsymbol{u}_o'> \tag{2}$$

where $<\ldots>$ represents a temporal average and $(\ldots)'$ represents temporal fluctuations about that average. Superscript "Rey" denotes Reynolds averaging. The second equality in Eq. 2 follows from a property specific to Reynolds averaging, $<<\ldots>>=<\ldots>$, which does not hold for more general decompositions such as coarse graining or a running window time average (*28*).

A negative value for EP^{Cg} or EP^{Rey} would indicate that wind is extracting energy from the eddy component of the flow, i.e., it indicates eddy killing. Consistent with previous studies, we shall show that the traditional measure EP^{Rey}, which is based on a temporal scale decomposition, is generally positive and fails to capture eddy killing. In contrast, we will show that our quantity EP^{Cg}, based on a spatial scale decomposition, is generally negative, consistent with physical expectations.

Unraveling eddy killing

The map in Fig. 2A is, to our knowledge, the first direct measurement of eddy killing in the global ocean, in which eddies encompass any flow structure associated with a length scale rather than temporal fluctuations or isolated coherent vortices. It results from our coarse-graining analysis of the wind stress, $\boldsymbol{\tau}$, obtained from QuikSCAT satellite data and of surface ocean velocity, $\boldsymbol{u}_o$, obtained from AVISO satellite altimetry data. We find eddy killing to be 50 GW globally, which is the power extracted by wind from the ocean at length scales smaller than 260 km. We also find the total power input by wind into the ocean, without any decomposition, to be 0.920 TW globally, in agreement with (*18*, *19*).

Figure 2A shows that eddy killing is occurring almost everywhere in the ocean including near the equator, except for positive values near some continental boundaries where small-scale currents are mostly wind-driven (*16*, *18*, *19*). Eddy killing is pronounced in WBCs and the Antarctic Circumpolar Current (ACC).

Figure 2B shows how we unraveled the length scale ℓ = 260 km below which eddy killing is operating in the global ocean. It shows a scan of our measure EP_ℓ^{Cg} in Eq. 1 over an entire range of length scales ℓ to detect those scales at which eddy killing operates, in addition to its magnitude. This scan in scale is a key advantage of coarse graining not possible with Reynolds averaging. How can we understand such a plot?

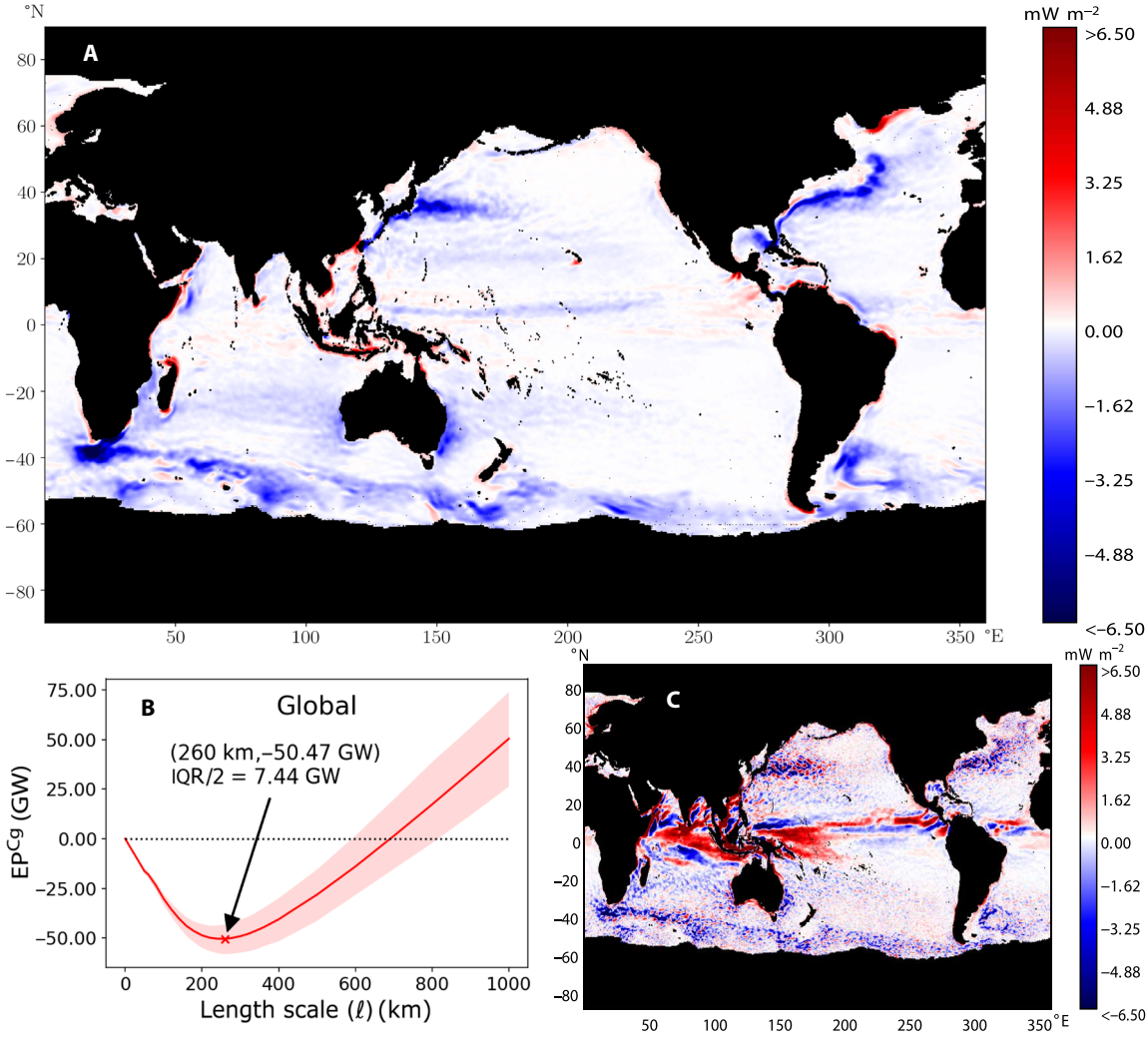

Fig. 2. Direct measurement of eddy killing by coarse graining. (**A**) Wind power input (in mW/m^2) to the flow at scales <260 km using our measure EP^{Cg} in Eq. 1. We are able to clearly detect eddy killing (negative values) throughout the global ocean, especially in WBCs and the Antarctic Circumpolar Current (ACC). Areas in black include land and ocean regions with seasonal or permanent ice coverage. (**B**) Performing a scan over an entire range of length scales to unravel scales at which eddy killing operates globally, in addition to its magnitude. This is a key advantage of coarse graining. At any scale ℓ, the plot shows wind power input to all scales smaller than ℓ. By attaining a minimum at ℓ = 260 km, it implies that eddies only at scales smaller than 260 km (but not larger) are losing energy to the wind, on average. Envelope shows interquartile range (IQR) (25th to 75th percentiles, *Q*1 to *Q*3) of temporal variation about the weekly climatology (as calculated from the 7 years of data) of EP_ℓ^{Cg}, and IQR/2 = (*Q*3 − *Q*1)/2. For reference, IQR/2 = 95.63 GW for the global $\tau \cdot u_o$ without any decomposition. (**C**) Reproducing eddy killing using the traditional Reynolds (or temporal) decomposition, EP^{Rey}, as had been done in prior studies. It shows a stark contrast to our measure EP^{Cg}, with sporadic values of mixed sign without a clear indication of eddy killing. The two decompositions differ starkly in the tropics but agree near some land boundaries, where we expect winds to drive small-scale currents.

The limit $\ell \to 0$ corresponds to a partitioning of length scales in which all belong to the "large scales," i.e., there is effectively no coarse graining and we retrieve the original (or "bare") flow (*29*, *30*). In this limit, we should have $\mathrm{EP}_\ell^{Cg} \to 0$ because there are no eddies, and all power is injected into the large scales, $\overline{\boldsymbol{\tau}} \cdot \overline{\boldsymbol{u}_o} = \boldsymbol{\tau} \cdot \boldsymbol{u}_o = 0.920$ TW, which is the total power injected by wind into the ocean without any decomposition.

The opposite extreme is when ℓ approaches the size of the domain such that coarse graining $\overline{(\cdots)}$ is effectively a spatial average over the entire ocean. This limit corresponds to all length scales, including basin-sized gyres, belonging to the eddies partition. In such a limit, we have the net power injected by wind into the ocean appearing as $\mathrm{EP}_\ell^{Cg} \approx \boldsymbol{\tau} \cdot \boldsymbol{u}_o$ (*29*). The limit $\ell \to \infty$ offers us a conceptual boundary condition on the plot in Fig. 2B, but its calculation requires convolutions that are too expensive (computational cost $\sim \ell^2$). The largest scale that we consider here is ℓ = 1000 km.

To summarize, by increasing the coarse-graining scale from ℓ = 0 to $\ell \to \infty$, we expect EP^{Cg}(ℓ = 0) = 0 to reach the net wind power input (a positive value) at very large filtering scales ℓ. However, this does not necessarily imply that EP^{Cg}(ℓ) increases monotonically in ℓ. Any dip in EP^{Cg}(ℓ) to a negative value would indicate eddy killing at scales <ℓ. This is precisely what is unraveled in Fig. 2B. In the Supplementary Materials, we provide an explanation for how the eddy killing scale is correlated with the spectral distribution of oceanic kinetic energy.

We see that EP_ℓ^{Cg} reaches a minimum value of −50.47 GW at scale ℓ = 260 km in Fig. 2B, which implies that eddies at scales smaller than 260 km are losing energy to the wind. What is the physical relevance of $EP^{Cg}(\ell = 260\ km)$ being a minimum? It implies that measuring EP_ℓ^{Cg} at a smaller partitioning scale, ℓ < 260 km, reduces the eddy killing magnitude because there are fewer eddy scales to be killed. It also implies that measuring EP_ℓ^{Cg} at a larger partitioning scale, ℓ > 260 km, reduces the eddy killing magnitude because those additional scales larger than 260 km (wind-driven currents, now lumped with eddies) have a net gain (rather than loss) of energy from the wind. Therefore, a minimum of EP_ℓ^{Cg} at scale ℓ = 260 km indicates that, on the global average, all scales smaller than 260 km are being killed by wind and scales larger than 260 km are gaining energy from the wind.

Such a result from decomposing wind power input into different length scales is nontrivial. Without a scale decomposition, we can only measure the net wind power input, $\boldsymbol{\tau} \cdot \boldsymbol{u}_o$ = 920 GW. Figure 2B allows us to appreciate that the wind feeds ≈970 GW to oceanic scales larger than 260 km, while it extracts ≈50 GW from oceanic scales smaller than 260 km. This insight has immediate relevance to general circulation models of varying resolution. We can also see from the envelope in Fig. 2B that eddy killing has relatively low temporal variability compared to wind power input at large scales. The net input of 920 GW to the global ocean has large temporal variability (SD of 173 GW), which is mostly at large length scales according to our analysis here. We shall present more evidence below that eddy killing is persistent in time.

In contrast to Fig. 2A, Fig. 2C shows how eddy killing cannot be captured by the Reynolds averaging approach traditionally used in oceanography. This is because a temporal analysis can fail to disentangle the inherent physics of eddy killing, which is spatial. A temporal analysis conflates all available spatial scales that constitute the temporal fluctuations, which (i) include large length scales that fluctuate in time and (ii) exclude small length scales that are steady. Both (i) and (ii) contribute to the unclear signal in Fig. 2C, which shows sporadic values of mixed sign without an obvious indication of eddy killing. Positive values dominate, falsely suggesting positive power input into the eddies. Globally, EP^{Rey} = + 38 GW, and if we exclude the ±3° equatorial band, then EP^{Rey} = + 13 GW, which is consistent with previous studies using the Reynolds decomposition (*18*, *19*). The positive values appearing in Fig. 2C are mostly absent from Fig. 2A, especially in the tropics and in the Indian Ocean. There is qualitative agreement, however, between Fig. 2 (A and C) in the positive values near some continental boundaries due to the small-scale wind-driven currents.

Significance of eddy killing

Our result that eddy killing removes a mere ≈5% (50 GW) of the total wind input globally (920 GW) may suggest that it is insignificant in the global budget. Yet, this indicates only that wind drives the large-scale (>260 km) flow much more strongly than it kills the mesoscales (<260 km)—a necessary condition for the existence of a wind-driven general circulation. Because it is widely appreciated that the mesoscales are a crucial (and most energetic) component of the oceanic circulation, it is thus more pertinent to compare eddy killing to other energy pathways in/out of the mesoscales.

It was estimated by (*31*, *32*) that ≈100 GW enters the eddies from the mean flow. A 50 GW in eddy killing is half that input from the mean flow. In the Gulf Stream, Kang and Curchitser (*33*) estimated that eddies are driven at a rate of ≈10 GW due to barotropic instabilities and ≈9 GW due to baroclinic instabilities. Here, we find that winds remove a substantial fraction of that energy, ≈ −5 GW due to eddy killing (see Table 1). Similarly in the Kuroshio, Yan *et al.* (*34*) estimated that eddies are driven at a rate of ≈6 GW due to barotropic instabilities and ≈18 GW due to baroclinic instabilities, compared to the eddy killing rate of ≈ −5 GW that we find here.

A coarse-graining analysis of the cascade that is more consistent with our result here was done in (*26*). From that study, we can estimate that in the ocean's top 100 m, kinetic energy leaves the mesoscales to larger scales at a rate ≈3.5 mW/m^2 in the Gulf Stream and ≈0.26 mW/m^2 in the entire North Atlantic. In comparison, eddy killing removes mesoscale energy at a rate ≈2 mW/m^2 in the Gulf Stream and ≈0.15 mW/m^2 globally (Table 1). Therefore, our estimates suggest that eddy killing is a mesoscale sink ≈60% of the strength of the inverse cascade pathway in the top 100 m of the ocean.

Regional trends

We shall now show that in dynamic regions of the ocean, eddy killing removes a large fraction of the wind power input. We show this by repeating our scan of EP_ℓ^{Cg} in scale, but now averaged over regions of interest.

We are able to determine the eddy killing length scale and magnitude at these locations in Fig. 3, where plots of EP_ℓ^{Cg} as a function of ℓ show a minimum at ℓ = 300 to 360 km in extratropical regions of interest. This implies that eddy killing is operating at scales smaller than ≈300 km (see also fig. S7) in these regions and that larger scales are gaining energy from the wind, on average, rather than being killed. The eddy killing scale in dynamic regions is slightly larger than the global eddy killing scale of ℓ = 260 km and is probably due to a more intense upscale energy cascade in these energetic regions (*26*), yielding larger scales. Despite comprising a mere 7% of the ocean's area, we find in fig. S7 that the dynamic regions contribute 35 GW in magnitude when combined, accounting for a majority of

Table 1. Regional wind power input. Total wind power input (first column), seen as a culmination of feeding scales larger (second column) and smaller (third column) than 260 km. We see that eddy killing removes a large fraction (≈90% in Kuroshio and ≈50% in Gulf Stream) of wind power input in some of these regions. It is so strong in the Agulhas (−0.18 mW/m^2) that it renders total wind work negative (≈ −1 GW) despite the positive power +1.40 mW/m^2 fed into large scales. When weighted by the regional area (fourth column), we see that much (≈40%) of the global eddy killing takes place in the ACC.

Regions	Total wind input (mW/m^2)	$\langle[\bar{\tau} \cdot \overline{u_o}]\rangle$ (mW/m^2)	EP^{Cg} (mW/m^2)	EP^{Cg} (GW)
Gulf Stream	4.11	6.12	−2.01	−5.25
Kuroshio Extension	1.86	3.58	−1.71	−4.70
Agulhas	−0.18	1.40	−1.58	−6.75
Brazil Malvinas	5.40	6.62	−1.22	−2.91
ACC	13.84	15.10	−1.26	−22.37
Southern Ocean	7.23	7.69	−0.45	−30.92
Global	2.67	2.82	−0.14	−50.47

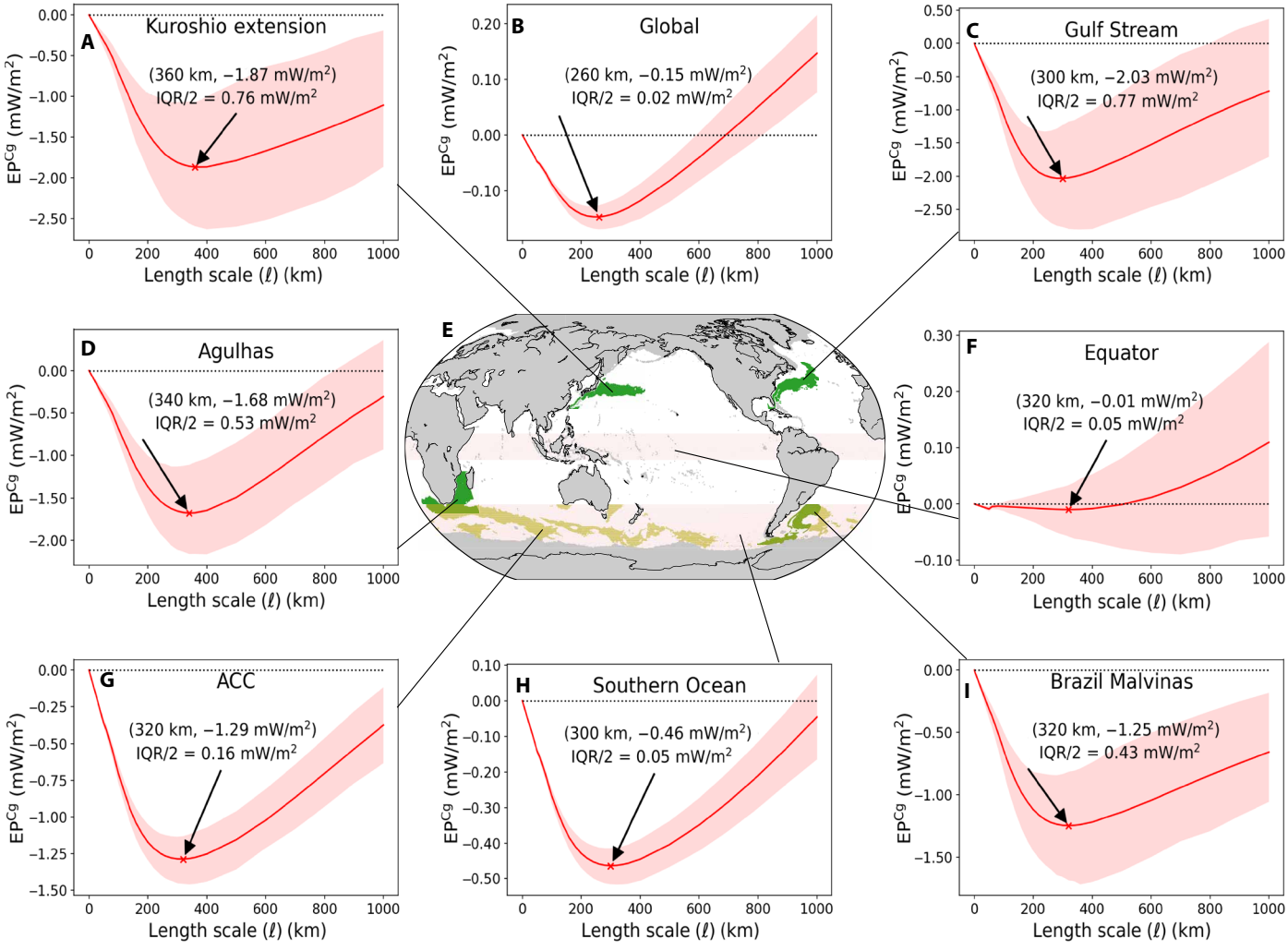

Fig. 3. Regional eddy killing. Similar to Fig. 2B for the global ocean, but restricted to regions of interest (see Materials and Methods), we scan our eddy killing measure EP^{Cg} as a function of length scale to unravel those scales at which eddy killing operates, in addition to its magnitude. We find that eddy killing occurs in most regions (**B** to **I**), except Kuroshio extension (**A**), at scales smaller than $\ell \approx 350$ km. The equatorial region of ±8° shows negligible eddy killing on average, with $EP^{Cg} \approx 0$ at scales $\ell < 500$ km and increasing almost monotonically without attaining a clear minimum.

the ocean's eddy killing, which occurs at scales smaller than 320 km. On the other hand, eddy killing in the remainder of the global ocean occurs at smaller scales <200 km, such that flow at larger scales tends to be wind-driven. This dilutes the global eddy killing average at 320 km and shifts it to slightly smaller scales of 260 km for the global average. We also find that the eddy killing scale generally decreases at higher latitudes (see fig. S8).

Unlike in our global analysis, eddy killing comprises a large fraction of overall wind power input in several of these regions (Table 1 and Fig. 3). In the Kuroshio, eddy killing as measured by $EP^{Cg}(\ell =$ 360 km) is approximately equal to (minus) the total power injected by the wind. Total power is positive only because the wind injects twice as much energy into scales larger than 360 km via $\overline{\boldsymbol{\tau}} \cdot \overline{\boldsymbol{u}_o}$. In the Gulf Stream, eddy killing is ≈50% of the total wind power injected in magnitude. In the Agulhas, eddy killing dominates the balance such that the total power injected is actually negative. Even with the wind feeding energy to scales larger than 340 km in the Agulhas, the intensity of eddy killing is such that on the whole (i.e., without any scale decomposition), wind extracts energy from the Agulhas circulation. We also find (see Table 1) that the Southern Ocean accounts for more than half (≈30 GW) of the global eddy killing.

Within the equatorial band ±8°, Fig. 3 shows that $EP^{Cg} \approx 0$ at scales $\ell < 500$ km and increases almost monotonically without attaining a clear minimum. This implies that the idealized eddy killing configuration sketched in Fig. 1 is unlikely to occur at the equator, where the flow is mostly wind-driven at scales smaller than ~1000 km. Figure S8 provides more insight; within ±8°, the westward trade winds oppose the eastward equatorial counter current and do indeed damp the flow at those large scales of $O(10^3)$ km, but this is not eddy killing in the sense implied in Fig. 1. This is also clear from Fig. 2A, which shows $EP^{Cg} \approx 0$ at the equator for $\ell = 260$ km, in stark contrast to the Reynolds averaging analysis in Fig. 2C.

Seasonality

Our results thus far have been time averaged over 7 years of data. How much variation and seasonality do eddy killing and large-scale

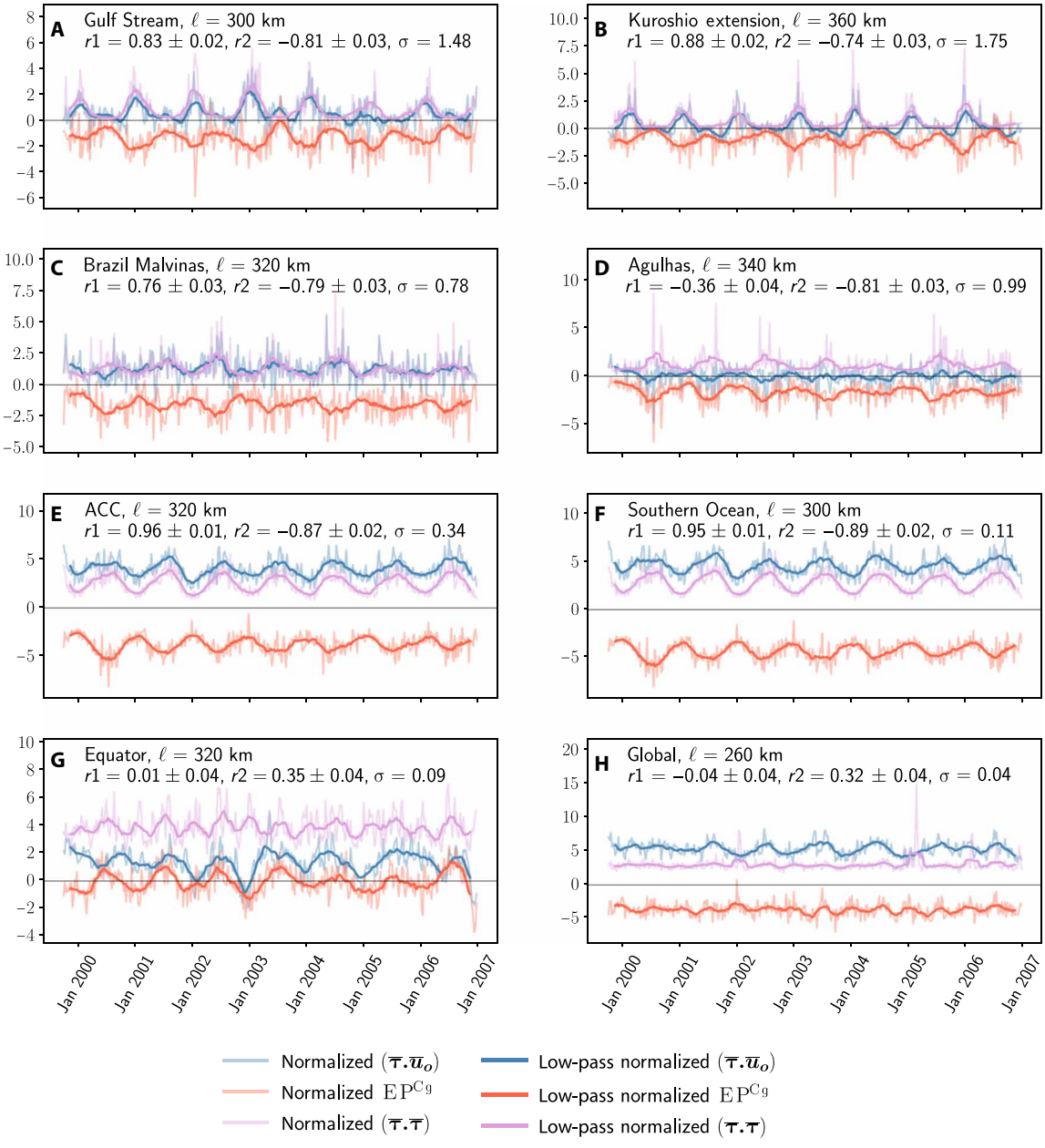

Fig. 4. Seasonality of eddy killing. Time series of wind power fed into scales larger (blue) and smaller (red) than the eddy killing scale ℓ shown in each panel (**A** to **H**), along with wind stress magnitude (purple). Thick line plots are a low-pass 91-day running average of the thin line plots. To allow for comparison, each time series $\phi(t)$ is normalized by its SD σ_ϕ: $\hat{\phi}(t) = \phi(t)/\sigma_\phi$. We see that eddy killing is persistent throughout the time series (red plots are negative), in all regions but the equator (G). Eddy killing (red) exhibits clear seasonal variation peaking in winter and tends to be anticorrelated with wind strength (purple). We offer an explanation in the Supplementary Materials (see eq. S-5 in the Supplementary Materials). Each panel also shows the SD of $\mathrm{EP}^{\mathrm{Cg}}$ (σ in mW/m^2) and two Pearson's correlation coefficients ["*r*1" between (thick) blue and purple plots and "*r*2" between (thick) red and purple plots with their 95% confidence intervals].

wind driving exhibit? Figure 4 plots the time series of wind power input into scales smaller and larger than the eddy killing scale, $\mathrm{EP}_\ell^{\mathrm{Cg}}$ and $\overline{\boldsymbol{\tau}} \cdot \overline{\boldsymbol{u}_o}$ respectively, in regions of interest and globally. We observe that throughout the 7-year series, there is persistent eddy killing ($\mathrm{EP}_\ell^{\mathrm{Cg}} < 0$) globally and also in all regions except the equator where $\mathrm{EP}^{\mathrm{Cg}} \approx 0$. Moreover, there is a clear seasonal variation with eddy killing peaking in winter. Large-scale wind driving also exhibits clear seasonality in the extratropics, generally peaking in the winter months. The seasonality of eddy killing is strongly correlated to that of wind strength, also shown in Fig. 4 to peak in winter. An explanation for this correlation is provided in the Supplementary Materials. Seasonal eddy killing was proposed by Zhai *et al.* (*35*) as a potential explanation for the seasonal cycle of eddy kinetic energy in the Gulf Stream. Our Fig. 4 provides direct evidence from observations in support of (*35*) that eddy killing contributes to mesoscale seasonality.

Using a new method of multiscale analysis of satellite data, we have unraveled the length scales at which eddy killing operates in the global ocean along with measuring its intensity. We have provided

direct evidence that eddy killing operates in the ocean at almost all times and peaks in winter. To our knowledge, such demonstration of the scale and temporal behavior of eddy killing has not been documented before. Traditional temporal analysis approaches used in previous work cannot detect the process of eddy killing as we have demonstrated here. Our results from satellites are also reinforced by analyzing a fully coupled 0. 1° Community Earth System Model (CESM) simulation shown in figs. S2 to S6.

Eddy killing constitutes a large fraction of the net wind power input in dynamic regions, even rendering the overall wind power input negative in the Agulhas current. Globally, eddy killing is an essential pathway to dissipation for the mesoscales, which are the most energetic component of the oceanic circulation and may play a leading role in its response to changes in atmospheric forcing and in the global transport of heat and biogeochemical tracers.

Our analysis here can be applied to future satellite altimetry and scatterometry data, which promise to be at higher resolution. The resolution of the current satellite data is unlikely to affect our eddy killing length scale result of 260 km, which we believe is well resolved. Yet, future datasets at higher resolution are likely to show that eddy killing is larger in magnitude than the 50-GW result that we find here.

Our results here reinforce emerging evidence (*16*, *36*) that a misrepresentation of eddy killing in models will most likely result in systematic biases in both the large and small scales and over short and long time forecasts. Our identification that wind feeds 970 GW into oceanic scales larger than 260 km and extracts 50 GW from smaller scales provides a practical and objective guide to current efforts at parameterizing this process in ocean models with varying grid resolution (*36*).

MATERIALS AND METHODS

Description of datasets

Geostrophic ocean surface velocity data on a 0.25° by 0.25° grid was obtained from satellite altimetry [AVISO Ssalto/Duacs, distributed by Copernicus Marine Environment Monitoring Service (CMEMS)]. The dataset includes estimates of geostrophic current along the equator using Lagerloef methodology (*37*) with the β-plane approximation.

Wind stress data on a 0.25° by 0.25° grid was obtained from the QuikSCAT satellite scatterometer distributed by PO.DAAC. Following the parameterization in (*18*, *38*), wind stress based on the QuikSCAT surface winds $\boldsymbol{u}_{qs}$ is given as

$$\boldsymbol{\tau} = \boldsymbol{u}_{qs} F(u_{qs}) \tag{3}$$

$$F(u_{qs}) = \alpha + \beta u_{qs} + \gamma {u_{qs}}^2 \tag{4}$$

where u_{qs} is the magnitude of $\boldsymbol{u}_{qs}$, and $\alpha = 2.70 \times 10^{-3} \rho_{air}$ (kg m^{-2} s^{-1}), $\beta = 1.42 \times 10^{-4} \rho_{air}$ (kg m^{-3}), and $\gamma = 7.64 \times 10^{-5} \rho_{air}$ (kg m^{-4} s). The air density used is $\rho_{air} = 1.223$ kg m^{-3}.

We carried out a 7-day running average on ascending and descending swaths after removing rain flagged data. We also carried out a 7-day running average on the ocean velocity data for consistency. The wind and current records used here extend from October 1999 to December 2006 and include ocean regions with seasonal ice coverage.

Because scatterometry measures the wind surface stress directly, $\boldsymbol{\tau}$ inherently accounts for the ocean's velocity relative to the wind and the dynamical feedback. An important requirement for our study is that the ocean and atmosphere are fully coupled and allow for a two-way feedback (*16*), which is also satisfied by the fully coupled CESM model used in the Supplementary Materials.

The satellite datasets that we use on a 0.25° grid are estimated to have an effective resolution that is two to four times coarser (*39*–*41*). However, the eddy killing length scale of 260 km is well resolved within our current analysis. A salient assumption that we make, similar to prior works (*18*, *19*, *23*, *25*), is that the sampling of (i) wind stress from QuikSCAT and (ii) current from altimetry are matched in space and time. While a potential mismatch can lead to an underestimation of eddy killing magnitude, these errors are not expected to be important over (time or length) scales greater than the resolution of the datasets.

Reynolds averaging

Reynolds averaging is a traditional approach that decomposes signals into temporal mean and fluctuating components. For our purposes, the mean wind stress and ocean surface current are $<\boldsymbol{\tau}>$ and $<xtbfu_o>$, respectively, where <…> represents temporal average over the entire data record.

Coarse graining

For a field $\phi(\boldsymbol{x})$, a "coarse-grained" or (low-pass) filtered field, which contains length scales larger than ℓ, is defined as

$$\overline{\phi}_\ell(\boldsymbol{x}) = G_\ell * \phi \tag{5}$$

where * is a convolution on the sphere (*27*) and $G_\ell(\boldsymbol{r})$ is a normalized kernel (or window function) so that $\int d^2\boldsymbol{r} G_\ell(\boldsymbol{r}) = 1$. Operation in equation 5 may be interpreted as a local space average over a region of diameter ℓ centered at point $\boldsymbol{x}$. The kernel G_ℓ that we use is essentially a graded Top-Hat kernel

$$G_\ell(r) = A(0.5 - 0.5\tanh((|\boldsymbol{r}| - \ell/2)/10.0)) \tag{6}$$

where $|\boldsymbol{r}|$ is geodesic distance. The normalizing factor A ensures $\int d^2\boldsymbol{r} G_\ell(r) = 1$.

Regional analysis

We generate masks for oceanic regions of interest shown in Fig. 3 over which we analyze eddy killing. The equatorial mask is the ±8° band, and the Southern Ocean mask is the (35° to 65°S) band. The remaining masks are irregular and are intended to select strongly eddying regions with strong currents. Specifically, the masks satisfy $\frac{1}{2}|<\boldsymbol{u}_o>|^2 + \frac{1}{2}<|\boldsymbol{u}_o'|^2> > 0.1$ m^2/ts^2 in the Gulf Stream and Kuroshio and $\frac{1}{2}|<\boldsymbol{u}_o>|^2 + \frac{1}{2}<|\boldsymbol{u}_o'|^2> > 0.05$ m^2/s^2 in the remaining regions shown in Fig. 3. Subject to these thresholds, the masks lie within [35° to 70°S] (ACC), [15° to 85°W and 23° to 55°N] (Gulf Stream), [120° to 180°E and 23° to 50°N] (Kuroshio), [0° to 45°E and 15° to 40°S] (Agulhas), and [40° to 75°W and 35° to 60°S] (Brazil-Malvinas).

SUPPLEMENTARY MATERIALS

Supplementary material for this article is available at http://advances.sciencemag.org/cgi/content/full/7/28/eabf4920/DC1

REFERENCES AND NOTES

1. C. Wunsch, R. Ferrari, Vertical mixing, energy, and the general circulation of the oceans. *Annu. Rev. Fluid Mech.* **36**, 281–314 (2004).

2. W. K. Dewar, G. R. Flierl, Some effects of the wind on rings. *J. Phys. Oceanogr.* **17**, 1653–1667 (1987).
3. X. Zhai, R. J. Greatbatch, Wind work in a model of the northwest Atlantic Ocean. *Geophys. Res. Lett.* **34**, 10.1029/2006GL028907, (2007).
4. M. M. Flexas, A. F. Thompson, H. S. Torres, P. Klein, J. T. Farrar, H. Zhang, D. Menemenlis, Global estimates of the energy transfer from the wind to the ocean, with emphasis on near-inertial oscillations. *J. Geophys. Res. Oceans* **124**, 5723–5746 (2019).
5. L. Renault, M. J. Molemaker, J. Gula, S. Masson, J. C. McWilliams, Control and stabilization of the Gulf Stream by oceanic current interaction with the atmosphere. *J. Phys. Oceanogr.* **46**, 3439–3453 (2016).
6. R. Ferrari, C. Wunsch, Ocean circulation kinetic energy: Reservoirs, sources, and sinks. *Annu. Rev. Fluid Mech.* **41**, 253–282 (2009).
7. C. Wunsch, D. Stammer, The global frequency-wavenumber spectrum of oceanic variability estimated from TOPEX/POSEIDON altimetric measurements. *J. Geophys. Res. Oceans* **100**, 24895–24910 (1995).
8. D. Stammer, Global characteristics of ocean variability estimated from regional TOPEX/POSEIDON altimeter measurements. *J. Phys. Oceanogr.* **27**, 1743–1769 (1997).
9. C. O. Dufour, S. M. Griffies, G. F. de Souza, I. Frenger, A. K. Morrison, J. B. Palter, J. L. Sarmiento, E. D. Galbraith, J. P. Dunne, W. G. Anderson, R. D. Slater, Role of mesoscale eddies in cross-frontal transport of heat and biogeochemical tracers in the Southern Ocean. *J. Phys. Oceanogr.* **45**, 3057–3081 (2015).
10. L. Mémery, G. Reverdin, J. Paillet, A. Oschlies, Introduction to the POMME special section: Thermocline ventilation and biogeochemical tracer distribution in the northeast Atlantic Ocean and impact of mesoscale dynamics. *J. Geophys. Rese. Oceans* **110**10.1029/2005JC002976, (2005).
11. V. C. Garçon, A. Oschlies, S. C. Doney, D. McGillicuddy, J. Waniek, The role of mesoscale variability on plankton dynamics in the North Atlantic. *Deep-Sea Res. II Top. Stud. Oceanogr.* **48**, 2199–2226 (2001).
12. R. Pacanowski, Effect of equatorial currents on surface stress. *J. Phys. Oceanogr.* **17**, 833–838 (1987).
13. J.-J. Luo, S. Masson, E. Roeckner, G. Madec, T. Yamagata, Reducing climatology bias in an ocean–atmosphere CGCM with improved coupling physics. *J. Climate* **18**, 2344–2360 (2005).
14. R. J. Small, K. J. Richards, S.-P. Xie, P. Dutrieux, T. Miyama, Damping of tropical instability waves caused by the action of surface currents on stress. *J. Geophys. Res. Oceans* **114**, 10.1029/2008JC005147, (2009).
15. L. Renault, J. C. McWilliams, J. Gula, Dampening of submesoscale currents by air-sea stress coupling in the Californian upwelling system. *Sci. Rep.* **8**, 10.1029/2008JC005147, (2018).
16. L. Renault, M. J. Molemaker, J. C. McWilliams, A. F. Shchepetkin, F. Lemarié, D. Chelton, S. Illig, A. Hall, Modulation of wind work by oceanic current interaction with the atmosphere. *J. Phys. Oceanogr.* **46**, 1685–1704 (2016).
17. L. Renault, P. Marchesiello, S. Masson, J. C. Mcwilliams, Remarkable control of western boundary currents by Eddy Killing, a mechanical air-sea coupling process. *Geophys. Res. Lett.* **46**, 2743–2751 (2019).
18. C. W. Hughes, C. Wilson, Wind work on the geostrophic ocean circulation: An observational study of the effect of small scales in the wind stress. *J. Geophys. Res. Oceans* **113**, 10.1029/2007JC004371, (2008).
19. R. B. Scott, Y. Xu, An update on the wind power input to the surface geostrophic flow of the World Ocean. *Deep-Sea Res. I Oceanogr. Res. Pap.* **56**, 295–304 (2009).
20. T. H. Duhaut, D. N. Straub, Wind stress dependence on ocean surface velocity: Implications for mechanical energy input to ocean circulation. *J. Phys. Oceanogr.* **36**, 202–211 (2006).
21. Y. Xu, R. B. Scott, Subtleties in forcing eddy resolving ocean models with satellite wind data. *Ocean Model.* **20**, 240–251 (2008).
22. D. K. Hutchinson, A. M. C. Hogg, J. R. Blundell, Southern Ocean response to relative velocity wind stress forcing. *J. Phys. Oceanogr.* **40**, 326–339 (2010).
23. C. Xu, X. Zhai, X.-D. Shang, Work done by atmospheric winds on mesoscale ocean eddies. *Geophysical Research Letters* **43**, (2016).
24. H. Seo, A. J. Miller, J. R. Norris, Eddy–wind interaction in the California current system: Dynamics and impacts. *J. Phys. Oceanogr.* **46**, 439–459 (2016).
25. L. Renault, J. C. McWilliams, S. Masson, Satellite observations of imprint of oceanic current on wind stress by air-sea coupling. *Sci. Rep.* **7**, 17747 (2017).
26. H. Aluie, M. Hecht, G. K. Vallis, Mapping the energy cascade in the North Atlantic Ocean: The coarse-graining approach. *J. Phys. Oceanogr.* **48**, 225–244 (2018).
27. H. Aluie, Convolutions on the sphere: Commutation with differential operators. *GEM Int. J. Geomathematics* **10**, 9 (2019).
28. M. Germano, Turbulence: The filtering approach. *J. Fluid Mech.* **238**, 325–336 (1992).
29. H. Aluie, Coarse-grained incompressible magnetohydrodynamics: Analyzing the turbulent cascades. *New J. Phys.* **19**, 025008 (2017).
30. G. L. Eyink. Review of the Onsager "Ideal Turbulence" Theory (2018);arXiv.org.
31. J.-S. von Storch, C. Eden, I. Fast, H. Haak, D. Hernández-Deckers, E. Maier-Reimer, J. Marotzke, D. Stammer, An estimate of the Lorenz energy cycle for the world ocean based on the STORM/NCEP simulation. *J. Phys. Oceanogr.* **42**, 2185–2205 (2012).
32. R. Chen, G. R. Flierl, C. Wunsch, A description of local and nonlocal Eddy–Mean Flow Interaction in a global eddy-permitting state estimate. *J. Phys. Oceanogr.* **44**, 2336–2352 (2014).
33. D. Kang, E. N. Curchitser, Energetics of eddy–mean flow interactions in the Gulf Stream region. *J. Phys. Oceanogr.* **45**, 1103–1120 (2015).
34. X. Yan, D. Kang, E. N. Curchitser, C. Pang, Energetics of eddy-mean flow interactions along the western boundary currents in the North Pacific. *J. Phys. Oceanogr.* **49**, 789–810 (2019).
35. X. Zhai, R. J. Greatbatch, J.-D. Kohlmann, On the seasonal variability of eddy kinetic energy in the Gulf Stream region. *Geophys. Res. Lett.* **35**, L24609 (2008).
36. L. Renault, S. Masson, T. Arsouze, G. Madec, J. C. Mcwilliams, Recipes for how to force oceanic model dynamics. *J. Adv. Model. Earth Syst.* **12**, e2019MS001715 (2020).
37. G. S. E. Lagerloef, G. T. Mitchum, R. B. Lukas, P. P. Niiler, Tropical Pacific near-surface currents estimated from altimeter, wind, and drifter data. *J. Geophys. Res. Oceans* **104**, 23313–23326 (1999).
38. W. G. Large, J. C. McWilliams, S. C. Doney, Oceanic vertical mixing: A review and a model with a nonlocal boundary layer parameterization. *Rev. Geophys.* **32**, 363–403 (1994).
39. M. R. Mazloff, S. T. Gille, B. Cornuelle, Improving the geoid: Combining altimetry and mean dynamic topography in the California coastal ocean. *Geophys. Res. Lett.* **41**, 8944–8952 (2014).
40. F. Desbiolles, A. Bentamy, B. Blanke, C. Roy, A. M. Mestas-Nuñez, S. A. Grodsky, S. Herbette, G. Cambon, C. Maes, Two decades [1992–2012] of surface wind analyses based on satellite scatterometer observations. *J. Mar. Syst.* **168**, 38–56 (2017).
41. D. Stammer, A. Cazenave, Eds., *Satellite Altimetry Over Oceans and Land Surfaces* (CRC Press, 2017).
42. G. L. Eyink, Locality of turbulent cascades. *Physica D* **207**, 91–116 (2005).
43. M. Sadek, H. Aluie, Extracting the spectrum of a flow by spatial filtering. *Phys. Rev. Fluids* **3**, 124610 (2018).
44. R. J. Small, J. Bacmeister, D. Bailey, A. Baker, S. Bishop, F. Bryan, J. Caron, J. Dennis, P. Gent, H.-m. Hsu, M. Jochum, D. Lawrence, E. Muñoz, P. diNezio, T. Scheitlin, R. Tomas, J. Tribbia, Y.-H. Tseng, M. Vertenstein, A new synoptic scale resolving global climate simulation using the Community Earth System Model. *J. Adv. Model. Earth Syst.* **6**, 1065–1094 (2014).
45. C. Wunsch, The work done by the wind on the oceanic general circulation. *J. Phys. Oceanogr.* **28**, 2332–2340 (1998).
46. J.-S. Von Storch, H. Sasaki, J. Marotzke, Wind-generated power input to the deep ocean: An estimate using a 1/10 general circulation model. *J. Phys. Oceanogr.* **37**, 657–672 (2007).

Acknowledgments: We thank M. Buzzicotti, M. Sadek, and B. Storer for valuable discussions and B. Storer for help with the statistical analysis. We also thank the reviewers for their careful reading and insightful suggestions. **Funding:** This research was funded by U.S. NASA grant 80NSSC18K0772 and a grant from LANL's Center for Space and Earth Science. H.A. was also supported by U.S. DOE grants DE-SC0014318, DE-SC0020229, and DE-SC0019329; NSF grant PHY-2020249; and U.S. NNSA grants DE-NA0003856 and DE-NA0003914. Computing time was provided by NERSC under contract no. DE-AC02-05CH11231 and NASA's HEC Program through NCCS at Goddard Space Flight Center. **Author contributions:** S.R. carried out all the data analysis and wrote the first manuscript draft. H.A. conceived of the initial idea and analysis method. All authors contributed to the interpretation of the results and writing of the manuscript. **Competing interests:** The authors declare that they have no competing interests. **Data and materials availability:** All data needed to evaluate the conclusions in the paper are present in the paper and/or the Supplementary Materials. The data underlying our analysis can be downloaded from CMEMS at https://resources.marine.copernicus.eu/?option=com_csw&task=results?option=com_csw&view=details&product_id=SEALEVEL_GLO_PHY_L4_REP_OBSERVATIONS_008_047 and from PO.DAAC at https://podaac-opendap.jpl.nasa.gov/opendap/allData/quikscat/L3/jpl/v2/hdf/.

Submitted 30 October 2020
Accepted 25 May 2021
Published 7 July 2021
10.1126/sciadv.abf4920

Citation: S. Rai, M. Hecht, M. Maltrud, H. Aluie, Scale of oceanic eddy killing by wind from global satellite observations. *Sci. Adv.* **7**, eabf4920 (2021).

Scale of oceanic eddy killing by wind from global satellite observations

Shikhar Rai, Matthew Hecht, Matthew Maltrud and Hussein Aluie

Sci Adv **7** (28), eabf4920.
DOI: 10.1126/sciadv.abf4920